Steady State EB Cap Size Fluctuations are Determined by Stochastic Microtubule Growth and Maturation

Jamie Rickman[1,2], Christian Duellberg[1,3], Nicholas I. Cade[1], Lewis D. Griffin[2], Thomas Surrey[1,#]

[1] The Francis Crick Institute, 1 Midland Road, London, NW1 1AT, United Kingdom

[2] Centre for Mathematics and Physics in Life Sciences and Experimental Biology (CoMPLEX), University College London, Gower Street, London, WC1E 6BT, United Kingdom

[3] Present address: Institute of Science and Technology Austria, Am Campus 1, 3400 Klosterneuburg, Austria

corresponding author: thomas.surrey@crick.ac.uk

ABSTRACT

Growing microtubules are protected from depolymerisation by the presence of a GTP or GDP/Pi cap. Proteins of the EB1 family bind to the stabilising cap allowing monitoring of its size in real time. The cap size has been shown to correlate with instantaneous microtubule stability. Here we have quantitatively characterised the properties of cap size fluctuations during steady state growth, and have developed a theory predicting their timescale and amplitude from the kinetics of microtubule growth and cap maturation. In contrast to growth speed fluctuations, cap size fluctuations show a characteristic timescale which is defined by the lifetime of the cap sites. Growth fluctuations affect the amplitude of cap size fluctuations; however, cap size does not affect growth speed, indicating that microtubules are far from instability during most of their time of growth. Our theory provides the basis for a quantitative understanding of microtubule stability fluctuations during steady state growth.

INTRODUCTION

The dynamic nature of the microtubule cytoskeleton is essential for its function: it allows for fast adjustments and reorganisations of the internal cell architecture depending on the state of the cell and its environment[1-3]. At the heart of this dynamicity is the propensity of microtubules to switch stochastically between phases of growth and shrinkage, called dynamic instability[4-6]. GTP hydrolysis by lattice-incorporated tubulin is ultimately responsible for this behaviour[7, 8]. After addition of tubulin to the growing microtubule end, GTP hydrolysis and phosphate release occur only after a delay. Hence GTP-tubulins are enriched in the microtubule end region, forming a protective cap that stabilises the growing microtubule[1, 9, 10].

Although details are still debated, the fast transition from growth to shrinkage, called catastrophe, is thought to be triggered by the loss of the GTP cap, likely as a consequence of stochastic fluctuations in its size[4, 9, 11, 12]. The exact properties of these cap size fluctuations are unknown because the GTP in the growing microtubule end region cannot be directly visualised. However, end binding proteins of the EB family have been shown recently to bind to the protective cap[13-16]. Fluorescent EBs can therefore be used to indirectly visualise the cap at the individual microtubule level[14].

These studies revealed that the cap consists of hundreds of tubulins in the stabilising conformation and that they have a roughly mono-exponential distribution starting from the growing microtubule end, giving rise to the comet-shaped appearance of the EB binding region[13, 15, 17, 18]. The majority of this EB cap is lost during a period of several seconds before catastrophe occurs[16, 19], indicating that the EB binding region is critical for stability. In agreement with this notion, faster growing microtubules which have larger caps were found to be more stable after sudden tubulin removal[14]. During regular steady state growth, cap size and microtubule stability appeared to fluctuate on a time scale of several seconds[14], the origin of which is unclear.

In the simplest kinetic model, cap sites are generated by tubulin incorporation into the microtubule lattice followed by a growth speed independent maturation process that forms the mature lattice[13, 19, 20]. Maturation corresponds to a conformational change, most likely associated with GTP hydrolysis or phosphate release[15, 16, 19, 21]. The maturation rate can be experimentally determined from the characteristic length of the EB binding region and the average microtubule growth speed, a procedure called 'comet analysis'[13, 19, 22].

As freshly added tubulins can also dissociate from microtubule ends, the net tubulin incorporation rate is the difference between the tubulin association and dissociation rates[23-27]. Therefore, in the simplest scenario only three rates - the tubulin association, dissociation and maturation rate - might be sufficient to describe the kinetic network of the formation of the protective cap (Fig. 1a).

The quantitative investigation of microtubule growth fluctuations, using mean-squared displacement (MSD) analysis, revealed large growth fluctuations, suggesting fast association and

dissociation kinetics[23, 28]. However, despite their presumed importance for microtubule stability, the fluctuations of the protective cap size have not yet been measured. Their properties, such as their typical amplitude and characteristic timescale, are unknown and it is unclear if cap size fluctuations can contribute to growth fluctuations.

Intrinsic network noise has been extensively studied for gene expression and other biochemical networks[29-34]. The specific properties of the noise were often found to be of functional importance. Moreover, chemical network theory has demonstrated that the fluctuation properties of a network are determined by its topology and reaction rates.

Here, we develop a theory that predicts the fluctuation characteristics of the protective cap during microtubule growth from a simple kinetic network of cap formation. Using correlation analysis, we measured for the first time the properties of the cap size fluctuations using EBs as a cap size marker and compared them to the measured properties of the growth fluctuations. We find that, in agreement with theory, growth fluctuations can be considered as Gaussian white noise and cap size fluctuations are well described by the mean-reverting Ornstein-Uhlenbeck (OU) process[35-37] with a typical timescale that is determined entirely by the maturation rate. This explains the timescale of previously observed stability fluctuations during microtubule growth[14]. Furthermore, the expected and measured amplitude of the cap size fluctuations indicates that microtubules are far from instability during most of their growth time. Overall, the agreement between theory and experiment suggests that the basic properties of the fluctuations in the size of the protective cap can be explained using a simple kinetic model.

THEORY

The cap reaction network

We assume a single protofilament kinetic model for microtubule growth and cap formation summarised by the following scheme and illustrated in Figure 1a.

$$\emptyset \underset{k_d}{\overset{k_a}{\rightleftarrows}} C \xrightarrow[k_m]{} L$$

The cap, C, grows by the addition of GTP-bound subunits to the microtubule end with an association rate k_a, which is proportional to the tubulin concentration. The cap shrinks by two processes: (i) the dissociation of subunits from the microtubule end, which occurs at a constant rate independent of the cap size, and (ii) depletion via maturation of cap sites into lattice sites, L, at rate $k_m n$ where k_m is the maturation rate constant and n is the number of cap sites. For simplicity this model neglects a recently reported pre-maturation step. This step is considerably faster than the maturation step, especially in the presence of EB1 proteins, making the pre-EB1 binding region much smaller than the EB binding region[19].

Time-averaged properties of the network

Previous studies[13, 19, 22, 23] have demonstrated how the three kinetic rate constants of the cap reaction network can be derived from the time-averaged properties of two observables: the growth trajectory of the microtubule and the spatial distribution of its cap sites. The growth trajectory represents a 1D Brownian 'diffusion-with-drift' process with mean growth speed and diffusion constant given by[23] $v_g = (k_a - k_d)\, a$ and $D = \frac{1}{2}(k_a + k_d)\, a^2$, respectively. Here a is the length of a subunit in the single protofilament model, considered to be the length of a tubulin dimer (8 nm) divided by 13 (the typical number of protofilaments in a microtubule).

From 'comet analysis' (Methods), the spatial probability distribution is given by[19] $\langle P(x,t)\rangle = e^{-\frac{x}{l}}$, where $P(x,t)$ is equal to 1 (0) if the subunit at position x, measured from the terminal subunit, is a cap site (lattice site). The maturation rate k_m can be obtained from the growth speed v_g and the average comet length l, since $l = \frac{v_g}{k_m}$. The average number of subunits in the cap, μ, is then given by l/a:

$$\mu = (k_a - k_d)/k_m\,. \tag{1}$$

Fluctuation properties of the network

Growth velocity fluctuations

From the definition of Brownian motion the length increments of the microtubule represent independent identically distributed Gaussian random variables. In the linear noise approximation[33] (LNA) we can define velocity fluctuations by $v(t) = \frac{L(t+\Delta t)-L(t)}{\Delta t}$ ($L(t+\Delta t)-L(t)$ is a length increment over time interval Δt) and write $v(t) = v_g + \xi_v(t)$, where $\xi_v(t)$ is a Gaussian white noise term accounting for the stochasticity of the microtubule growth[30, 32]. Setting $\Delta t = 1$, the power in the noise term is proportional to the sum of the rates of the two Poisson processes of association and dissociation[11]: $\langle \xi_v(t)\xi_v(t')\rangle = (k_a + k_d)\, a^2\, \delta(t-t')$. The autocovariance function (ACF) of the velocity fluctuations is then given by:

$$C_v(\tau) = (k_a + k_d)\, a^2 \delta(\tau). \tag{2}$$

$\delta(\tau)$ is the Dirac delta function. The form of this ACF reflects the 'memorylessness' of the growth fluctuations i.e. there is no characteristic timescale. The zero lag magnitude reveals the fluctuation amplitude:

$$\sigma_v = \sqrt{k_a + k_d}\, a. \tag{3}$$

Cap size fluctuations

In the cap reaction network the size of the cap fluctuates about its mean value driven away from equilibrium by growth fluctuations. Following a perturbation the cap reverts back to its mean size via the maturation process on a characteristic 'relaxation' timescale τ; this is the 'mean-reverting' property of the OU process.

To find the ACF of the cap size fluctuations we can write a deterministic equation for the evolution of the cap: $\dot{n}(t) = k_a - k_d - k_m n$. In the LNA we perturb this expression about its mean and again add a noise term; $\delta\dot{n}(t) = -k_m\, \delta n(t) + \xi_c(t)$, to get an expression for the stochastic fluctuations. The Gaussian noise term, $\xi_c(t)$, is the sum of a component due to the growth fluctuations, $\xi_v(t)$, and an independent component due to the maturation step, $\xi_m(t)$, characterised by[32]; $\langle \xi_m(t)\, \xi_m(t') \rangle = k_m \langle n \rangle\, \delta(t - t')$. With these expressions the ACF of the cap size fluctuations can be obtained (see SI Appendix, SI Methods for details):

$$C_c(\tau) = \frac{k_a}{k_m} e^{-k_m \tau}. \tag{4}$$

The maturation rate enters here as the inverse of the relaxation time, characterising the memory of the fluctuations. The zero lag magnitude reveals the fluctuation amplitude:

$$\sigma_c = \sqrt{k_a / k_m}\,. \tag{5}$$

Cross-correlation of growth velocity and cap size fluctuations

The cross-covariance function (CCF) can also be found from the above expressions (see SI Appendix, SI Methods for details), it is given by:

$$C_{vc}(\tau) = \frac{1}{a} {\sigma_v}^2 e^{-k_m \tau}\, U(\tau). \tag{6}$$

$U(\tau)$ is the unit step function. The asymmetry of the CCF results from causality in the network; the growth fluctuations drive the cap size fluctuations but there is no feedback from cap to growth[38].

Measurement noise

In the presence of experimental measurement noise, modeled as white Gaussian noise, the ACFs require additional terms (see SI Appendix, SI Methods for details). The ACF of the velocity fluctuations becomes;

$$C'_v(\tau) = {\sigma_v}^2 \delta(\tau) + \Gamma_v^2 \big(2\delta(\tau) - \delta(\tau - \Delta t)\big), \tag{7}$$

and the ACF of the cap size fluctuations becomes;

$$C'_c(\tau) = {\sigma_c}^2 e^{-k_m \tau} + \Gamma_c^2\, \delta(\tau). \tag{8}$$

Γ_v^2 and Γ_c^2 denote the squared amplitude of the position and cap size measurement noise respectively.

RESULTS

To measure the properties of EB cap size fluctuations, microtubules were grown from surface-immobilized GMPCPP-stabilized seeds in the presence of purified Alexa568-tubulin and GFP-tagged fission yeast EB1 (Mal3) (Fig. 1b), essentially as described[13, 39] (Methods). Experiments were performed at three different tubulin concentrations. Microtubule growth and EB cap size fluctuations were monitored using dual-colour time-lapse total internal reflection fluorescence (TIRF) microscopy,

with an image acquisition rate of 4 frames s^{-1} (Fig. 1c). The growing plus ends of microtubules were tracked[16, 40, 41], and the corresponding intensity of the EB1-GFP signal in the microtubule end region was recorded using an automated procedure[19] (Methods). For analysis, we considered only continuous growth episodes of at least 200 s duration (Methods and SI Appendix Fig. S2), excluding catastrophe episodes.

Cap formation kinetics from time-averaged data

First, we extracted the time-averaged characteristics of the observed steady state growth trajectories. Representative trajectories show visible fluctuations with faster growth at higher tubulin concentration, as expected (Fig. 1d). Mean growth speeds were determined by MD analysis (Fig. 1d-middle, SI Appendix, SI Methods) and the diffusion constant was quantified with MSD analysis (Fig. 1d-bottom, SI Appendix, SI Methods), characterising the diffusion-with-drift process. From the MSD analysis an estimate for the positional measurement noise was also obtained. From the estimates of the diffusion constant and the mean growth speed the tubulin association and dissociation rates can be derived, which were found to be large compared to their difference (SI Appendix, Fig. S1), in agreement with the notion of fast assembly kinetics[23, 42]. The average EB cap length at plus ends was extracted from time-averaged EB1-GFP intensity profiles (Fig. 1e) by comet analysis[13, 14, 19]. From the mean growth speeds and the comet lengths the maturation rates were derived (Methods). The time-averaged properties of the cap reaction network are summarised in Fig. 1f.

Properties of velocity fluctuations

Next we used fluctuation analysis to study the growth fluctuations directly. We obtained velocity time series by calculating finite differences of the microtubule positions at 2 Hz (Methods). Representative velocity traces show that the velocities fluctuate randomly over time (Fig. 2a) resulting in Gaussian-shaped velocity distributions (Fig. 2b), as expected. We then calculated the ACF of the velocity traces (Fig. 2c, Methods). The increasing magnitude of the ACFs at the origin with increasing tubulin concentration reflects the expected larger fluctuation amplitudes (intrinsic noise) with growth speed due to faster association and dissociation kinetics (equation (3)), as also seen in the broadening of the velocity distributions (Fig. 2b). Measurement noise also contributes to the magnitude at the origin and causes the negative correlation at the shortest time lag (equation (7)). Estimates of the intrinsic noise and measurement noise were extracted from the ACFs (Methods, Fig. 2d). Their combined values agreed well with sigma values of Gaussian fits to the velocity distributions (Fig. 2b, d), demonstrating consistency. The measurement noise was in the expected range of the microtubule end tracking precision[40]. In further agreement with theory, the absence of a characteristic correlation time reflects the Poissonian nature of the association and dissociation of tubulin at growing microtubule ends.

The velocity fluctuation amplitude can also be predicted from the results of MSD analysis (Methods) and compared to the fluctuation analysis results. Measurement noise estimates can be

compared directly. Good agreement confirms the close mathematical relationship between these two methods (Fig. 2e, f). However the fluctuation analysis goes further by explicitly showing that the velocity fluctuations are 'memoryless', supporting the model of microtubule growth as a Brownian diffusion-with-drift.

Properties of EB cap size fluctuations

To measure directly the properties of the EB cap size fluctuations we analysed time series of EB1-GFP intensities in the microtubule end region. As expected from theory (equation (1)) representative time traces (Fig. 3a) and histograms of EB1-GFP intensities (Fig. 3b) show that the mean intensity, corresponding to the total cap size, increases with tubulin concentration i.e. growth speed[13]. Also in agreement with theory (equation (5)) the amplitudes of the fluctuations increase with tubulin concentration (Fig. 3a, b). Interestingly, the intensity fluctuations give the impression of a strong low frequency structure, which was not seen in the velocity fluctuations (Fig. 2a).

We computed ACFs of the EB cap intensity fluctuations and found that in contrast to the velocity fluctuations they showed an apparently mono-exponential decay on a timescale of several seconds (Fig. 3c). The loss of some correlation within the first time lag is the expected consequence of white Gaussian measurement noise (equation (8)). As a control we also analysed the Alexa568-tubulin intensity in the microtubule end region; ACFs revealed that in addition to the measurement noise signature, a slowly decaying correlation was detectable beyond the first time lag (Fig. 3d). This correlated noise was present in both fluorescence channels as demonstrated by cross-covariance analysis (SI Appendix, Fig. S3a, b) and was therefore contributing to the measured ACF (SI Appendix, Fig. S3c). It is likely the consequence of thermal motion of the microtubules in the z-direction of the sample ('microtubule wiggling'), expected to occur at this timescale[43], leading to slow intensity fluctuations due to the exponentially decaying profile of the TIRF evanescent field in the z-direction[44].

Therefore, we performed a mono-exponential fit to the ACF of the Alexa568-tubulin intensity fluctuations and a bi-exponential fit to the ACF of the EB cap size fluctuations sharing the decay time corresponding to microtubule wiggling (Methods). The shorter decay time of the bi-exponential fit gives an estimate of the maturation rate, k_m ($1/\tau$). Extracted τ values were in the same range for all tubulin concentrations: 5.0 ± 1.1 s, 8.1 ± 1.2 s and 4.8 ± 0.5 s for 10 μM, 20 μM and 30 μM tubulin, respectively. These values agree well with those obtained from comet analysis (Fig. 1f, Fig. 3e), providing independent support for our simple model and confirming that the maturation rate is essentially independent of the microtubule growth velocity[13, 20], as expected theoretically.

Next we determined the mean size of the EB cap and the amplitude of the cap size fluctuations from the ACFs of the EB fluorescence intensity time traces (Fig. S4a, b, Methods). We found again that both the mean cap size and the fluctuation amplitude increased with tubulin concentration, i.e. with growth velocity, consistent with theory (equations (1) and (5)). The mean cap

size increases from 266 subunits at 10 μM to 736 subunits at 30 μM (Fig. 3f) implying a cap of 20-60 tubulin layers long (since 13 tubulin subunits comprise a layer) for our range of experimental conditions. This is in agreement with earlier estimates for microtubules growing in vitro[13, 14, 19] and in living cells[18]. Over the same range of tubulin concentrations, the amplitude of the fluctuations increased from 64 to 178 subunits (Fig. 3g).

The mean cap size and its fluctuation amplitude can also be predicted from the analysis of time-averaged data, i.e. of spatial EB intensity profiles ('comets'), MD and MSD plots (Methods); good agreement between the time-averaged analysis and the fluctuation analysis further supports the theory (Fig. 3f, g). These results provide the first quantitative characterisation of the properties of EB cap size fluctuations and their dependence on microtubule growth velocity.

Cross-correlation of growth speed and cap size fluctuations

The topology of the cap reaction network defines a direction of causality: microtubule growth fluctuations affect cap size fluctuations but cap size fluctuations do not influence growth fluctuations. For such a model, one expects a distinct CCF as shown by simulated data (Fig. 4b). We computed the average CCFs between the measured growth fluctuations and cap size fluctuations for the three tubulin concentrations (Fig. 4c). The mixing of two noisy signals resulted in relatively noisy cross-covariance curves. Nevertheless all curves clearly show an asymmetry with exponential decays on the side of positive time lags and roughly zero covariance at negative time lags, in qualitative agreement with theory (equation (6)). These observations further support the topology of the reaction network and the derived theory for steady state microtubule growth velocity and cap size fluctuations.

DISCUSSION

Here we have measured the fluctuations in the size of the protective cap of growing microtubules using fluorescent EB proteins as cap markers. Using correlation analysis we have characterised the properties of these fluctuations and have found that the amplitude and characteristic timescale of the cap size fluctuations can be understood quantitatively based on a simple kinetic reaction network describing cap formation. Theoretical expressions for the properties of the fluctuations have been derived using concepts from chemical network analysis, previously applied in studies of gene expression and other biochemical networks[29-31]. The measured timescale and amplitude of the cap size fluctuations agreed quantitatively with values predicted with kinetic rates obtained from time-averaged data (comet and MSD analysis), demonstrating consistency.

Interestingly, the cap size fluctuations show very different characteristics compared to the growth velocity fluctuations. This is due to the nature of the underlying chemical kinetic processes. Growth speed fluctuations are determined by two Poisson processes, tubulin association and dissociation[23, 26], whereas cap size fluctuations are additionally determined by cap site maturation, most likely the transformation of GTP (or GDP/Pi) tubulin to GDP tubulin[15, 16, 21]. The instantaneous

rate of cap site maturation depends linearly on the fluctuating cap size, resulting in a process formally similar to diffusion in a potential well (Ornstein-Uhlenbeck process). The cap represents a 'mean-reverting' system characterised by the timescale at which it relaxes back to its average size following a stochastic perturbation, which is the inverse of the characteristic frequency i.e. the maturation rate constant. The relatively slow kinetics of cap site maturation limits the response of the cap size to the fast growth fluctuations and effectively attenuates the high frequency perturbations caused by the stochastic growth.

We can now explain the timescale of microtubule stability fluctuations, as previously observed in tubulin washout experiments[14]. In these experiments, faster growing microtubules with larger protective caps were more stable[14]. However, the correlation between instantaneous microtubule stability and cap size was lost when they were measured several seconds apart[14], which is indeed in the range of the characteristic timescale of the cap size fluctuations, as shown here. Hence, the maturation time in the range of seconds as shown here (Fig. 1e, Fig. 3e) and elsewhere[13-15, 19, 20] sets the timescale of instantaneous microtubule stability fluctuations. This timescale also eliminates EB1 binding dynamics as a significant source of EB1 fluctuations: for the experimental conditions here, these dynamics occur on a ~100 millisecond scale and would only contribute a few percent variation (SI Appendix, SI Methods).

The observed asymmetry of the cross-covariance function of growth velocity and cap size fluctuations indicate that in a steady growth state, velocity fluctuations drive cap size fluctuations, but not vice versa. Whereas this supports the topology of the simple kinetic reaction network of cap generation, it may also appear surprising, because the mean cap size decreases strongly over several seconds before catastrophe[16, 19], suggesting that cap size could affect growth speed. However, here we excluded catastrophe episodes and growth pauses from our analysis, as we wanted to focus on steady state growth alone. In fact, the observed cross-covariance function shows that microtubules are remarkably stable, for most of their time in steady state growth. Together with recent observations of a stability threshold being in the range of 10-30% of the average cap size[16, 19, 14] the amplitudes of cap size fluctuations as measured here and predicted by our theory, indicate that this stability threshold is indeed far from the mean cap size (~ 3 sigma).

Typical microtubule lifetimes at steady state are in the range of several 100 s, hence much longer than the maturation time[24, 25, 45-49]. How these two timescales are linked is currently unclear. Currently, no agreement exists yet as to what exactly the criterion inducing catastrophe is. Simple cap models have been criticized for not correctly describing the measured dependence of steady state microtubule lifetimes on their growth speed[50]. Finer detail on the structure of the cap, potentially influenced by the nanoscale structure of the microtubule end itself, such as the tapered or sheet-like extensions observed by electron microscopy[48] may have to be considered[51] for a more comprehensive model. Furthermore, defects[45] or lattice cracks[52-54] have been hypothesised to exist and to provide alternative or additional constraints on microtubule stability[45, 50, 53, 54]. Unfortunately, in contrast to the

cap size fluctuations, the real time observation of these other features is currently not possible, limiting direct tests of these models.

Our quantitative understanding of the properties of the protective cap size fluctuations during steady state growth, as developed here, will likely be useful in the future for the refinement of existing models and possibly the development of new quantitative models explaining the lifetime of microtubules based on the kinetic processes of growth and cap maturation, as well as for their regulation by accessory proteins.

MATERIALS AND METHODS

Microtubule dynamics assay. Microtubule plus end growth and the GFP intensity of fission yeast EB1 (Mal3-GFP) in the plus end region were measured in flow cells assembled as described previously[39] using TIRF microscopy [19, 55]. Alexa568-labelled microtubules were assembled from biotinylated, Alexa568-labelled and GMPCPP-stabilized seeds, which were attached to a functionalised glass coverslips via Neutravidin (Life Technologies). The free tubulin concentration was 10, 20 or 30 μM (of which 12.5 % was labelled with Alexa568 (Life Technologies)). For all experiments, Mal3-GFP was present at 200 nM. Simultaneous imaging of the Alexa568 channel and the GFP channel was performed at 4 Hz with an exposure time of 100 ms per frame and identical laser settings for all conditions. All experiments were performed at 30 ºC. More details can be found in the SI Appendix, SI Methods.

Automated microtubule tracking. For MSD analysis and fluctuation analysis of the microtubule growth, time traces of microtubule plus-end positions were extracted from the Alexa568 channel using a previously described MATLAB program, which has been shown to achieve sub-pixel resolution[19, 41]. Details can be found in the SI Appendix, SI Methods.

Processing tracks and selecting growth episodes. The extracted end positions occasionally showed some artefacts due to tracking errors. To mitigate the effects of these errors the tracks were further processed, as described in the SI Appendix, SI Methods and Figure S2. Furthermore, in the growth trajectories of the microtubules short episodes of very slow growth were also observed, reminiscent of 'pauses' of growth. We considered these growth episodes to be deviations from steady state behaviour and not applicable to our analysis of steady state growth. These episodes were removed from the data and the remaining partial tracks were subsequently considered separately. More details and statistics of these procedures are summarised in the SI Appendix, Table S1.

The remaining trajectories and their corresponding EB1 intensity fluctuation data were considered as representing pure steady state growth behaviour recorded with the highest possible positional tracking precision our automated tracking routine can deliver.

MSD analysis. Details of the MD and MSD analysis can be found in the SI Appendix, SI Methods.

EB1 comet analysis. Average EB1-GFP fluorescence intensity profiles (comets) of the growing microtubule end were generated and fitted with a convolved mathematical function to determine the average size of the EB cap and the maturation rate k_m. More details can be found in the SI Appendix, SI Methods.

Generation of velocity time series. We generated velocity time series by calculating finite differences of the position time series at 2 Hz (half the image acquisition rate). Thus two time series were generated for each track, one from even numbered frames and one from odd numbered frames. Velocities were not calculated at the smallest possible time difference to reduce the relative magnitude of the measurement noise. The two resulting time series were considered separately, consistent with the theoretical analysis that treats microtubule length increments (equivalently velocity fluctuations) as independent.

Correlation analysis. Details of calculating ACFs can be found in the SI Appendix, SI Methods.

Analysis of velocity autocovariance functions and comparison to MSD analysis. Mean velocity autocovariance functions are plotted for each tubulin concentration in Fig. 2c. An estimate for measurement noise was obtained from the magnitude of the correlation at the shortest time lag, which was compared directly to the estimate obtained from MSD analysis. The amplitude of the velocity fluctuations was obtained from the magnitude of the correlation at zero lag and the previously obtained estimate of the measurement noise (equation (7)), this was compared to the estimate of the fluctuation amplitude derived from MSD analysis since (setting $\Delta t = 1$) $\sigma_v^2 = 2D$.

Analysis of the EB1-GFP autocovariance functions. As a control we calculated the normalised ACFs of the Alexa568-tubulin channel and found there was a slowly decaying correlation revealing a source of correlated noise present in the fluorescence intensity measurements (Fig. 3d), which is likely due to thermal fluctuations of the microtubule[43]. Cross-correlation analysis confirmed that the same external noise source was affecting the EB1-GFP intensity measurements (SI Appendix, Fig. S3a, b). The EB1-GFP ACFs therefore comprise a component from the EB1-GFP fluctuations and also a component from the correlated noise. To account for this we performed a global fit to the six curves in Fig. 3c & d, as described in SI Appendix, SI Methods.

Calculating mean cap size and cap fluctuation amplitude from intensity measurements. From the time-averaged analysis (MSD and comet analysis) estimates of D, v_g and k_m were obtained. We used these results to calculate averages values for the mean cap size, μ, (equation (1)) and the squared

cap size fluctuation amplitude, σ^2, (equation (5)) for each tubulin concentration. The same properties, in fluorescence units rather than numbers of cap sites, can be calculated from the fluctuation analysis of EB1-GFP intensities. We then converted the fluorescence intensity measurements into numbers of cap sites and made a direct comparison (Fig. 3f, g). More details are given in the SI Appendix, SI Methods and Figure S4.

Simulation of cross-correlation. A full stochastic simulation of the cap reaction network developed from a previous study[24] was used to test the validity of our model and the robustness of our analysis to experimentally limiting factors. 20 simulated tracks of 200s long were analysed to replicate our experimental data sets. We tested our analysis under a range of simulated noise conditions (modeled as additive white Gaussian noise) covering what was measured experimentally. We also analysed simulated data at 4 Hz and a faster rate of 10 Hz (SI Appendix, Fig. S4). We found the simulation results fitted the theory well in all cases. Example simulation data and cross-correlation analysis results are shown in Fig. 4a & b.

ACKNOWLEDGEMENTS

We thank Philippe Cluzel for hosting TS in his lab for two weeks and for helpful discussions, and Gunnar Pruessner for suggestions for data analysis. This work was supported by the Francis Crick Institute which receives its core funding from Cancer Research UK (FC001163), the UK Medical Research Council (FC001163), and the Wellcome Trust (FC001163). C.D. and T.S. were also supported by the European Research Council (Advanced Grant, project 323042).

AUTHOR CONTRIBUTIONS

JR, CD, NIC and TS designed the study. JR developed the theory and the corresponding methods of data analysis. CD designed and carried out the experiments and performed the automated microtubule end tracking. MSD and fluctuation analysis was performed by JR. Comet analysis and other image analysis was carried out by NIC. LDG provided computational and mathematics expertise. TS and JR wrote the manuscript with input from the co-authors.

COMPETING FINANCIAL INTERESTS

The authors declare no competing financial interests.

REFERENCES

1. Desai, A. & Mitchison, T.J. Microtubule polymerization dynamics. *Annu Rev Cell Dev Biol* **13**, 83-117 (1997).

2. Kumar, P. & Wittmann, T. +TIPs: SxIPping along microtubule ends. *Trends Cell Biol* **22**, 418-428 (2012).
3. Akhmanova, A. & Steinmetz, M.O. Control of microtubule organization and dynamics: two ends in the limelight. *Nat Rev Mol Cell Biol* (2015).
4. Mitchison, T. & Kirschner, M. Dynamic instability of microtubule growth. *Nature* **312**, 237-242 (1984).
5. Cassimeris, L., Pryer, N.K. & Salmon, E.D. Real-time observations of microtubule dynamic instability in living cells. *J Cell Biol* **107**, 2223-2231 (1988).
6. Horio, T. & Hotani, H. Visualization of the dynamic instability of individual microtubules by dark-field microscopy. *Nature* **321**, 605-607 (1986).
7. Hyman, A.A., Salser, S., Drechsel, D.N., Unwin, N. & Mitchison, T.J. Role of GTP hydrolysis in microtubule dynamics: information from a slowly hydrolyzable analogue, GMPCPP. *Mol Biol Cell* **3**, 1155-1167 (1992).
8. Caplow, M., Ruhlen, R.L. & Shanks, J. The free energy for hydrolysis of a microtubule-bound nucleotide triphosphate is near zero: all of the free energy for hydrolysis is stored in the microtubule lattice. *J Cell Biol* **127**, 779-788 (1994).
9. Carlier, M.F. Guanosine-5'-triphosphate hydrolysis and tubulin polymerization. Review article. *Mol Cell Biochem* **47**, 97-113 (1982).
10. Carlier, M.F. Nucleotide hydrolysis in cytoskeletal assembly. *Curr Opin Cell Biol* **3**, 12-17 (1991).
11. Howard, J. & Hyman, A.A. Growth, fluctuation and switching at microtubule plus ends. *Nat Rev Mol Cell Biol* **10**, 569-574 (2009).
12. Brouhard, G.J. Dynamic instability 30 years later: complexities in microtubule growth and catastrophe. *Mol Biol Cell* **26**, 1207-1210 (2015).
13. Bieling, P. *et al.* Reconstitution of a microtubule plus-end tracking system in vitro. *Nature* **450**, 1100-1105 (2007).
14. Duellberg, C., Cade, N.I., Holmes, D. & Surrey, T. The size of the EB cap determines instantaneous microtubule stability. *Elife* **5** (2016).
15. Maurer, S.P., Bieling, P., Cope, J., Hoenger, A. & Surrey, T. GTPgammaS microtubules mimic the growing microtubule end structure recognized by end-binding proteins (EBs). *Proc Natl Acad Sci U S A* **108**, 3988-3993 (2011).
16. Maurer, S.P., Fourniol, F.J., Bohner, G., Moores, C.A. & Surrey, T. EBs recognize a nucleotide-dependent structural cap at growing microtubule ends. *Cell* **149**, 371-382 (2012).

17. Bechstedt, S., Lu, K. & Brouhard, G.J. Doublecortin recognizes the longitudinal curvature of the microtubule end and lattice. *Curr Biol* **24**, 2366-2375 (2014).
18. Seetapun, D., Castle, B.T., McIntyre, A.J., Tran, P.T. & Odde, D.J. Estimating the microtubule GTP cap size in vivo. *Curr Biol* **22**, 1681-1687 (2012).
19. Maurer, S.P. *et al.* EB1 accelerates two conformational transitions important for microtubule maturation and dynamics. *Curr Biol* **24**, 372-384 (2014).
20. Bieling, P. *et al.* CLIP-170 tracks growing microtubule ends by dynamically recognizing composite EB1/tubulin-binding sites. *The Journal of Cell Biology* **183**, 1223-1233 (2008).
21. Zhang, R., Alushin, G.M., Brown, A. & Nogales, E. Mechanistic Origin of Microtubule Dynamic Instability and Its Modulation by EB Proteins. *Cell* **162**, 849-859 (2015).
22. Telley, I.A., Bieling, P. & Surrey, T. Reconstitution and quantification of dynamic microtubule end tracking in vitro using TIRF microscopy. *Methods Mol Biol* **777**, 127-145 (2011).
23. Gardner, M.K. *et al.* Rapid microtubule self-assembly kinetics. *Cell* **146**, 582-592 (2011).
24. Duellberg, C., Cade, N.I. & Surrey, T. Microtubule Ageing Probed by Microfluidics-Assisted Tubulin Washout. *Mol Biol Cell* (2016).
25. Walker, R.A. *et al.* Dynamic instability of individual microtubules analyzed by video light microscopy: rate constants and transition frequencies. *J Cell Biol* **107**, 1437-1448 (1988).
26. Schek, H.T., 3rd, Gardner, M.K., Cheng, J., Odde, D.J. & Hunt, A.J. Microtubule assembly dynamics at the nanoscale. *Curr Biol* **17**, 1445-1455 (2007).
27. Kerssemakers, J.W. *et al.* Assembly dynamics of microtubules at molecular resolution. *Nature* **442**, 709-712 (2006).
28. Reid, T.A. *et al.* Suppression of microtubule assembly kinetics by the mitotic protein TPX2. *J Cell Sci* **129**, 1319-1328 (2016).
29. Eldar, A. & Elowitz, M.B. Functional roles for noise in genetic circuits. *Nature* **467**, 167-173 (2010).
30. Ozbudak, E.M., Thattai, M., Kurtser, I., Grossman, A.D. & van Oudenaarden, A. Regulation of noise in the expression of a single gene. *Nat Genet* **31**, 69-73 (2002).
31. Levine, E. & Hwa, T. Stochastic fluctuations in metabolic pathways. *Proc Natl Acad Sci U S A* **104**, 9224-9229 (2007).

32. Komorowski, M., Miekisz, J. & Stumpf, M.P. Decomposing noise in biochemical signaling systems highlights the role of protein degradation. *Biophys J* **104**, 1783-1793 (2013).
33. Elf, J. & Ehrenberg, M. Fast evaluation of fluctuations in biochemical networks with the linear noise approximation. *Genome Res* **13**, 2475-2484 (2003).
34. Walczak, A.M., Mugler, A. & Wiggins, C.H. Analytic methods for modeling stochastic regulatory networks. *Computational Modeling of Signaling Networks*, 273-322 (2012).
35. Uhlenbeck, G.E. & Ornstein, L.S. On the theory of the Brownian motion. *Physical Review* **36**, 823 (1930).
36. Ricciardi, L.M. & Sacerdote, L. The Ornstein-Uhlenbeck process as a model for neuronal activity. I. Mean and variance of the firing time. *Biol Cybern* **35**, 1-9 (1979).
37. Aalen, O.O. & Gjessing, H.K. Survival models based on the Ornstein-Uhlenbeck process. *Lifetime Data Anal* **10**, 407-423 (2004).
38. Granger, C.W.J. Investigating causal relations by econometric models and cross-spectral methods. *Econometrica: Journal of the Econometric Society* 424-438 (1969).
39. Bieling, P., Telley, I.A., Hentrich, C., Piehler, J. & Surrey, T. Fluorescence Microscopy Assays on Chemically Functionalized Surfaces for Quantitative Imaging of Microtubule, Motor, and +TIP Dynamics. *Methods Cell Biology* **95**, 555-580 (2010).
40. Bohner, G. *et al.* Important factors determining the nanoscale tracking precision of dynamic microtubule ends. *J Microsc* (2015).
41. Ruhnow, F., Zwicker, D. & Diez, S. Tracking single particles and elongated filaments with nanometer precision. *Biophys J* **100**, 2820-2828 (2011).
42. Castle, B.T. & Odde, D.J. Brownian dynamics of subunit addition-loss kinetics and thermodynamics in linear polymer self-assembly. *Biophys J* **105**, 2528-2540 (2013).
43. Gittes, F., Mickey, B., Nettleton, J. & Howard, J. Flexural rigidity of microtubules and actin filaments measured from thermal fluctuations in shape. *J Cell Biol* **120**, 923-934 (1993).
44. Axelrod, D., Thompson, N.L. & Burghardt, T.P. Total internal inflection fluorescent microscopy. *J Microsc* **129**, 19-28 (1983).
45. Gardner, M.K., Zanic, M., Gell, C., Bormuth, V. & Howard, J. Depolymerizing kinesins Kip3 and MCAK shape cellular microtubule architecture by differential control of catastrophe. *Cell* **147**, 1092-1103 (2011).

46. Odde, D.J., Cassimeris, L. & Buettner, H.M. Kinetics of microtubule catastrophe assessed by probabilistic analysis. *Biophys J* **69**, 796-802 (1995).
47. Janson, M.E., de Dood, M.E. & Dogterom, M. Dynamic instability of microtubules is regulated by force. *J Cell Biol* **161**, 1029-1034 (2003).
48. Chretien, D., Fuller, S.D. & Karsenti, E. Structure of growing microtubule ends: two-dimensional sheets close into tubes at variable rates. *J Cell Biol* **129**, 1311-1328 (1995).
49. Geyer, E.A. *et al.* A mutation uncouples the tubulin conformational and GTPase cycles, revealing allosteric control of microtubule dynamics. *Elife* **4**, e10113 (2015).
50. Bowne-Anderson, H., Zanic, M., Kauer, M. & Howard, J. Microtubule dynamic instability: a new model with coupled GTP hydrolysis and multistep catastrophe. *Bioessays* **35**, 452-461 (2013).
51. Coombes, C.E., Yamamoto, A., Kenzie, M.R., Odde, D.J. & Gardner, M.K. Evolving tip structures can explain age-dependent microtubule catastrophe. *Curr Biol* **23**, 1342-1348 (2013).
52. Flyvbjerg, H., Holy, T.E. & Leibler, S. Microtubule dynamics: Caps, catastrophes, and coupled hydrolysis. *Phys Rev E Stat Phys Plasmas Fluids Relat Interdiscip Topics* **54**, 5538-5560 (1996).
53. Margolin, G. *et al.* The mechanisms of microtubule catastrophe and rescue: implications from analysis of a dimer-scale computational model. *Mol Biol Cell* **23**, 642-656 (2012).
54. Li, C., Li, J., Goodson, H.V. & Alber, M.S. Microtubule dynamic instability: the role of cracks between protofilaments. *Soft Matter* **10**, 2069-2080 (2014).
55. Duellberg, C. *et al.* Reconstitution of a hierarchical +TIP interaction network controlling microtubule end tracking of dynein. *Nat Cell Biol* **16**, 804-811 (2014).
56. Quenouille, M.H. Notes on bias in estimation. *Biometrika* **43**, 353-360 (1956).
57. Li, X.R. *Probability, random signals, and statistics*. (CRC Press, 1999).

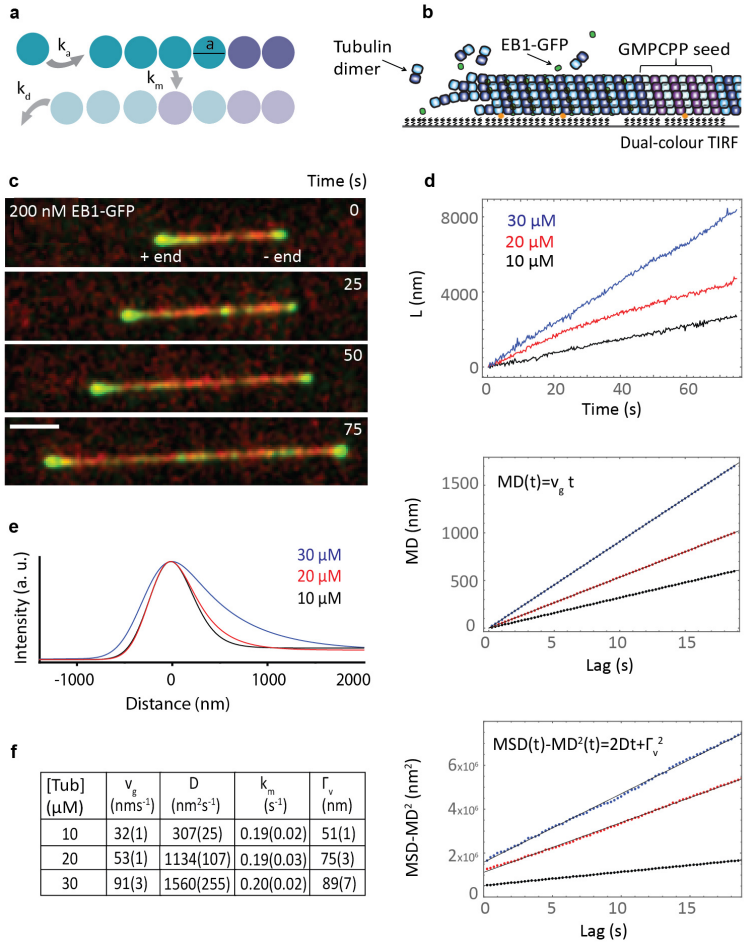

[Tub] (µM)	v_g (nms^{-1})	D (nm^{2}s^{-1})	k_m (s^{-1})	Γ_v (nm)
10	32(1)	307(25)	0.19(0.02)	51(1)
20	53(1)	1134(107)	0.19(0.03)	75(3)
30	91(3)	1560(255)	0.20(0.02)	89(7)

Figure 1. Microtubule growth and cap properties from time-averaged data. (a) Illustration of the single protofilament model with three kinetic rate constants for tubulin association (k_a), dissociation (k_d) and maturation (k_m). The length of a tubulin dimer a is 8/13 nm. **(b)** Schematic of the TIRF microscopy assay. **(c)** Image sequence from a representative dual-colour TIRF microscopy movie, acquired at a frame rate of 4 s^{-1} (scale bar: 3 µm). **(d)** (Top) Representative growth trajectories (position time traces) of microtubule plus ends for three tubulin concentrations as obtained by automated end tracking. (Middle) MD plotted over time calculated from 38, 25 and 17 growth trajectories with an average duration of 193 s, 196 s and 148 s for 10 µM, 20 µM, 30 µM tubulin, respectively. The mean growth speed v_g was extracted from fits to the data (black lines). (Bottom) Variance of the displacement (MSD minus MD squared) plotted over time. The diffusion constant, D, and the measurement noise, Γ_v, were extracted from fits to the data (black lines). **(e)** Time-averaged comet-shaped spatial EB1-GFP fluorescence intensity profiles were automatically generated from TIRF movies (with a total duration of 750 s, 1950 s and 1050 s of growth for increasing tubulin concentrations). The maturation rate constant k_m of the cap reaction network is obtained with comet analysis. **(f)** Table of mean growth speeds, diffusion constants, maturation rate constants and positional measurement noise estimates obtained from MD, MSD and comet analysis (errors given in brackets are SEM).

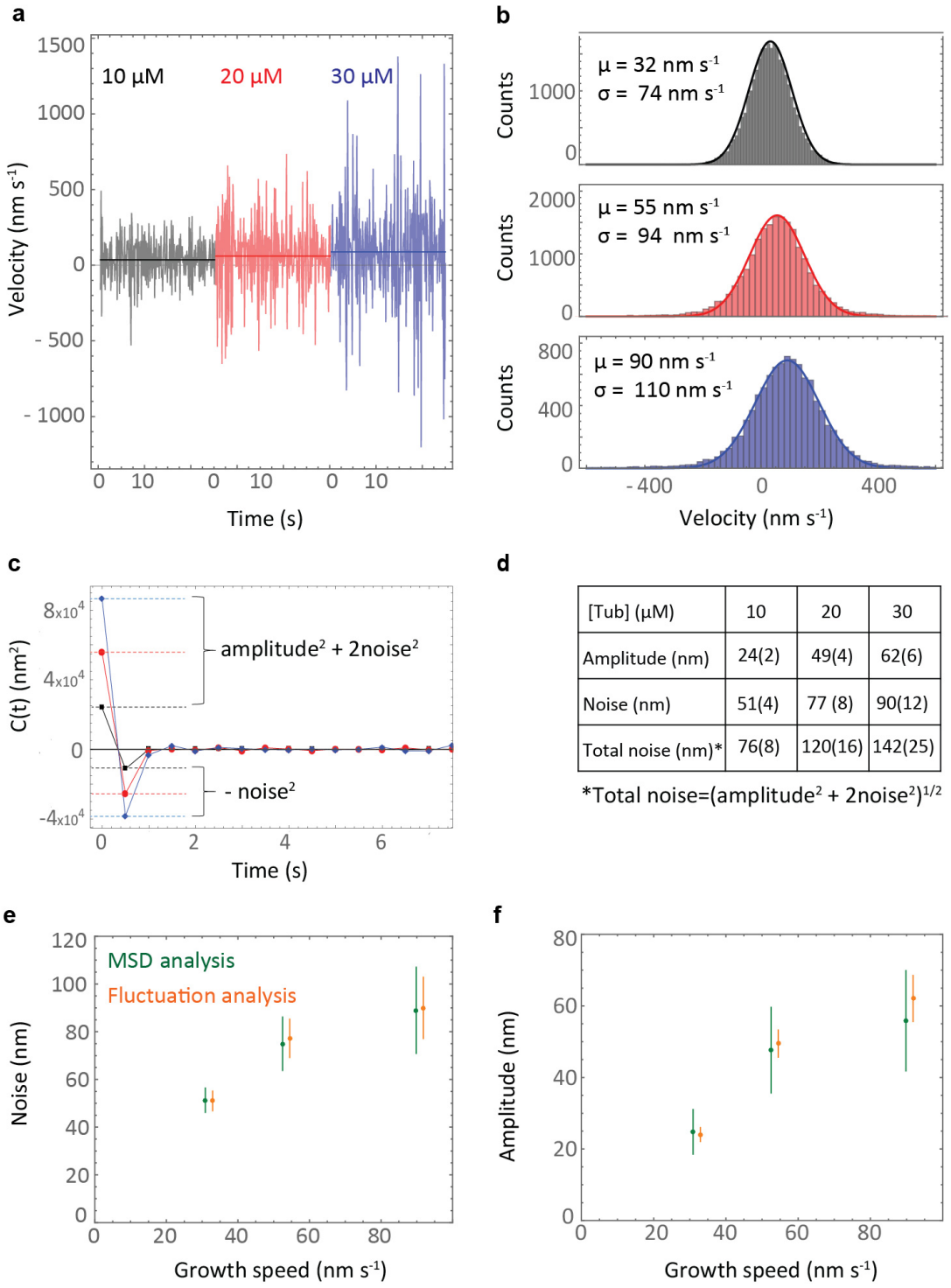

Figure 2. Fluctuation analysis of microtubule growth. (a) Representative velocity fluctuation traces generated from finite differencing the position data at 2 Hz. **(b)** Histograms of the velocity distributions show the average velocity and the standard deviation increase with tubulin concentration ($n = 1{\times}10^4, n = 2{\times}10^4, n = 3{\times}10^4$ with increasing tubulin concentration). **(c)** Plots of the average velocity ACF, indicative of Brownian diffusion in the presence of white Gaussian measurement noise. The magnitude at the origin increases with tubulin concentration due to larger growth fluctuations and higher measurement noise. Dashed lines indicate values extracted from the ACF. **(d)** Table of

parameter estimates extracted from the ACFs in (c). "Total noise" estimates that can be compared to the standard deviation of the Gaussian fits to the velocity histograms in (b). Errors in brackets are SEM. **(e) & (f)** Estimates of the amplitude of the growth fluctuations and the measurement noise obtained from the time-averaged analysis (MD and MSD) and the fluctuation analysis (ACFs) are compared (error bars: SEM), demonstrating good agreement between the two methods.

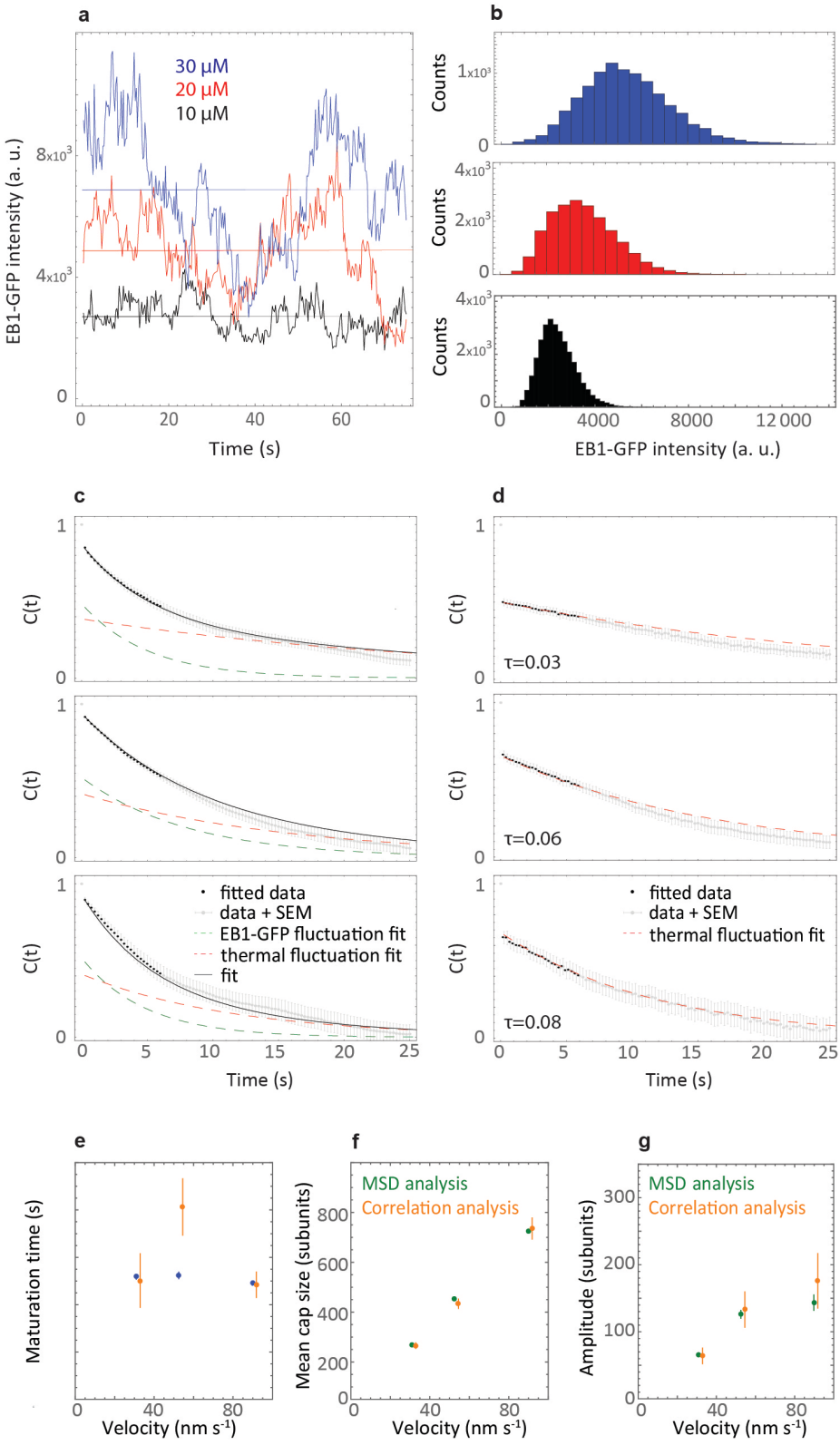

Figure 3. Fluctuation analysis of microtubule cap dynamics. (a) Representative time traces of the EB1-GFP fluorescence intensity fluctuations at growing microtubule ends for three tubulin concentrations. **(b)** Histograms of EB1-GFP intensity distributions show that the average signal and its standard deviation increase with tubulin concentration (*n* values as in Fig. 2b). **(c)** Normalised

ACF's of the EB1-GFP intensity fluctuations. **(d)** Normalised ACF's of the Alexa568-tubulin intensity fluctuations (error bars: SEM) revealing a source of correlated experimental noise. EB1-GFP intensity measurements are subject to the same correlated noise. Global fits (black lines) to pairs of ACF data (black dots) of tubulin (d) and EB1-GFP intensity (c) fluctuations (Methods, SI Appendix, Fig. S3c) produced estimates for decay rates due to EB1-GFP fluctuations (maturation rates) and correlated noise, respectively. **(e)** Comparison of maturation times ($k_m{}^{-1}$) from correlation analysis (d) and comet analysis (Fig. 1e). **(f) & (g)** The mean cap size and the amplitude of the cap size fluctuations were obtained from EB1-GFP intensity time traces and their normalised ACFs after finding a proportionality factor to convert fluorescence intensity into numbers of subunits (Methods). These values were compared to the same quantities derived from the time-averaged analysis (SI Appendix, Fig. S4 b&c) (error bars: SEM).

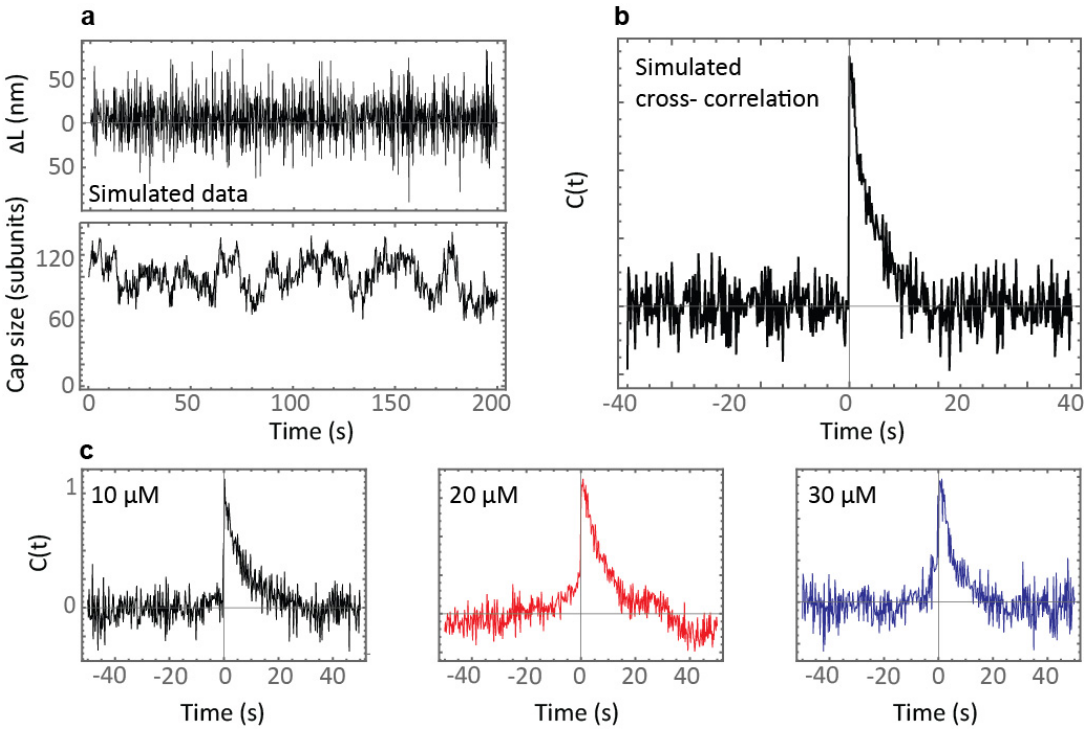

Figure 4. Cross-covariance analysis between growth speed and cap size fluctuations.

(a) An example microtubule length trajectory (top) and its cap size fluctuations (bottom) from a full stochastic simulation of the cap reaction network with added Gaussian noise replicating the experimentally measured noise levels. **(b)** Cross-covariance of simulated data (20 tracks, 200 s long) shows the expected one-sided exponential decay, demonstrating that growth fluctuations drive cap size fluctuations. **(c)** Experimental normalised cross-covariance functions show a strongly asymmetric shape and the apparent mono-exponential decays at positive lag times are in qualitative agreement with theory.